A Digital Predistortion System with Extended Correction Bandwidth with Application to LTE- A Nonlinear Power Amplifiers

Oualid Hammi, *Member*, *IEEE,* Andrew Kwan, *Graduate Student Member, IEEE,* Souheil Bensmida, *Member, IEEE*, Kevin A. Morris*, Member IEEE* and Fadhel M. Ghannouchi, *Fellow, IEEE*

Abstract—This article presents a bandwidth extended digital predistortion system suitable for LTE-advanced applications. The proposed predistortion system uses a two-box architecture based on the cascade of a memory polynomial followed by a memoryless predistortion function. The memoryless predistorter is identified offline and used to perform a coarse linearization which cancels out most of the static nonlinearity of the device under test allowing for a reduced observation bandwidth for the synthesis of the memory polynomial predistortion sub-function. The proposed predistorter was experimentally validated and its performance benchmarked against a predistorter having the same structure but identified using the conventional approach. The measurement results demonstrate that the proposed predistorter requires 30% less sampling speed for the analog to digital converter of the feedback path.

Index Terms—Analog to digital converter (ADC), digital predistortion (DPD), distortion, field programmable gate arrays, memory effects, nonlinearity, power amplifier (PA).

I. INTRODUCTION

RADIO frequency power amplifiers (PAs) are the main cause of nonlinearities in wireless transmitters. These nonlinearities appear as a result of using spectrum efficient modulation and multiplexing techniques such as multi-level quadrature amplitude modulation (QAM) and orthogonal frequency division multiplexing (OFDM), respectively. These techniques widely used in modern communication systems inevitably lead to amplitude modulated time domain signals with high peak-to-average power ratios (PAPR). To ensure power efficient operation of

the power amplification stage, architectures such as Doherty amplifiers and polar transmitters are adopted [1]-[7]. These power amplification circuits enhance the power efficiency while resulting in a substantially nonlinear behavior. In fact, the signal's amplitude modulation emulates the static nonlinear behavior of PAs. Moreover, dynamic distortions caused by the electrical memory effects will be induced due to the wide bandwidth of the signals to be transmitted. This calls for the use of linearization circuitry along with the power amplifier to reduce the spectral regrowth in the adjacent channels [8]-[16]. The predistortion technique is widely used for power amplifiers linearization, and can be implemented either in digital or in analog domains. Compared to digital predistorters, the analog implementation of the predistortion function yields to a much wider correction bandwidth but lower linearity performances [17][18]. Thus, digital predistortion (DPD) technique is the preferred choice for the linearization of base station power amplifiers. Several predistortion structures have been proposed to compensate for the dynamic nonlinear behavior of power amplifiers driven by wideband signals [10]-[16].

Digital predistortion is achieved by placing before the amplifier a complementary nonlinear function that will cancel out the distortions created by the PA. The performance of the digital predistorter is heavily dependent on the match between the predistortion function and the inverse characteristic of the PA. Accordingly, accurate characterization of the device under test is needed. This sets stringent bandwidth requirements since the signal at the output of a power amplifier is typically five times wider than the original signal to be transmitted [15][16]. In [15], a first attempt to address the wide bandwidth requirement of digital predistortion systems was reported. In this work, the band-limited approach consists of filtering the PA's output signal to limit the required observation bandwidth and applying a similar bandwidth limitation on the predistorted signal through filtering. This led to satisfactory linearization performance in the observation bandwidth but with no distortions correction beyond the observation bandwidth of the system. Recently, a DPD system able to reduce the spectrum regrowth over a bandwidth that exceeds the observation bandwidth was reported [16]. This is obtained by filtering the PA's output signal to alleviate the speed requirements on the analog to digital converters (ADC). The filtered spectral components are then recovered in the digital domain by using spectral extrapolation techniques which add

significant computational complexity to the DPD system.

In this paper, the bandwidth requirements of modern digital predistortion systems are addressed with two main objectives. The first aims at being able to reduce the spectral regrowth over a bandwidth that exceeds the observation bandwidth. The second objective is to avoid major additional computational overhead.

This paper is organized into five sections: Section II discusses the distributed dynamic nonlinearity approach adopted in this work. In Section III, the proposed bandwidth extended digital predistortion technique is described. The experimental validation of the proposed technique and its performance benchmarking are reported in Section IV. Section V concludes this article by summarizing the main results and deriving conclusions.

II. DISTRIBUTED DYNAMIC NONLINEARITY APPROACH

Two and three-box based digital predistorters have been widely investigated in the literature for the linearization of power amplifiers exhibiting memory effects [12]-[14]. The basic idea is that the nonlinearity order of the power amplifier is split into two lower order nonlinear functions. In fact, the cascade of two polynomial functions with nonlinearity orders K_1 and K_2, respectively, will result in a nonlinear system with nonlinear terms up to the $K_1 \times K_2$ order while requiring only $K_1 + K_2$ coefficients.

Accordingly, multi-box models demonstrated similar and even superior performance compared to single box models while requiring a lower number of coefficients [13][14]. When memory effects are present, a common approach consists of using a memoryless nonlinear function, that is optimized to compensate for the highly nonlinear memoryless characteristic of the device under test (DUT), and a dynamic function that compensates for the residual dynamic distortions of the device under test. The dynamic function is a linear filter in Wiener based predistorters, and a low order memory polynomial function in twin-nonlinear two-box models.

Fig. 1 presents the block diagram of the two-box digital predistorter considered in this work. It consists of the cascade of a dynamic nonlinear function followed by a static nonlinearity. The output signal of the dynamic nonlinearity block $\left(x_{interm}\right)$ built using a memory polynomial function is given by:

$$x_{interm}(i) = \sum_{n=0}^{N} \sum_{m=0}^{M} a_{nm} x(i-m) \left| x(i-m) \right|^n \qquad (1)$$

where N and M are the nonlinearity order and the memory depth of the memory polynomial function used to implement the dynamic nonlinearity of the predistorter, respectively.

Similarly, the output signal $\left(x_{out\_DPD}\right)$ of the static nonlinear predistorter is formulated according to:

$$x_{out\_DPD}(i) = \sum_{k=0}^{K} b_k x_{interm}(i) \left| x_{interm}(i) \right|^k \qquad (2)$$

where K refers to the nonlinearity order of the static nonlinearity sub-block of the proposed digital predistorter.

Substituting (1) into (2) will relate the predistorter's output signal $\left(x_{out\_DPD}\right)$ to its input signal $\left(x_{in}\right)$.
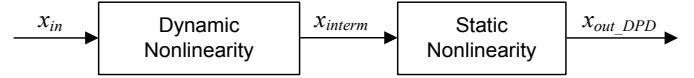

Fig. 1. Adopted two-box digital predistorter structure.

The predistorter of Fig. 1 is built according to the reverse twin-nonlinear two-box structure reported in [13]. However, the procedure used to identify the DPD coefficients in this work is very distinct from that of the original reverse twin-nonlinear two-box. This major difference enhances the bandwidth capability of the proposed predistorter which is explained in the next section. Separating the memoryless part (static nonlinearity) of the predistorter from its memory effects (dynamic nonlinearity) is a very attractive feature of the considered DPD. Indeed, it was shown, in [19], that the static distortion characteristics of the PA are more accurately measured under a narrow band test condition. This implies that the static nonlinearity of the digital predistorter structure shown in Fig. 2 can be derived from narrow band measurements.

Moreover, the specific cascaded arrangement of the adopted predistorter is suitable for implementing a two-step linearization process where the static nonlinear function of the DPD is first applied, and then the dynamic nonlinear function of the predistorter is synthesized to linearize the cascade made up of the memoryless DPD (static nonlinear function), and the device under test. This is achieved by using the signal $\left(x_{interm}\right)$ at the input of the static nonlinearity function and the sampled output of the device under test.

Furthermore, a closer look at the output spectra of the power amplifier before linearization, and after applying the memoryless DPD (built using the static nonlinearity function of the two-box DPD) reveals valuable information about the typical behavior of power amplifiers. Indeed, Fig. 2 illustrates a conceptual schematic that illustrates the impact of using a memoryless predistorter and a full two-box predistorter on the spectra at the output of the linearized amplifier. This figure shows that when only the static nonlinearity of the two-box DPD structure is applied to linearize the PA, substantial spectrum regrowth cancellation will be observed even if the amplifier exhibits strong memory effects. Most importantly, it is anticipated that the signal bandwidth at the output of the PA linearized using a memoryless DPD will be narrower than that obtained at the output of the PA without any predistortion. In fact, the static distortions are known to be highly nonlinear while memory effects are linear or at most mildly nonlinear [20][21]. Thus, when the static nonlinearity of the DUT is cancelled out by the memoryless DPD function, the bandwidth of the signal at the output of the PA will decrease. Consequently, the bandwidth of the feedback path and thus the ADC speed requirements can be reduced accordingly without compromising the quality of the linearization.
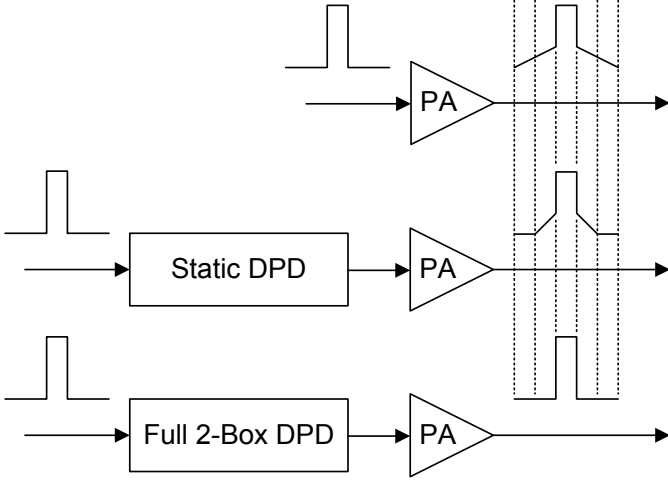
Fig. 2. Effects of various DPDs on the spectra at the output of a linearized PA.

III. BANDWIDTH EXTENDED DIGITAL PREDISTORTION TECHNIQUE

A conventional digital predistortion system is shown in Fig. 3. In the signal generation path, the signal to be transmitted (x_{in}) is first predistorted. The resulting signal at the output of the DPD is then converted by the digital to analog converter (DAC) before being upconverted by the frequency up-conversion stage (UCS). In the signal feedback path, a portion of the signal at the output of the power amplifier (x_{out_PA}) is down-converted by the down-conversion stage (DCS), and then digitized by the analog to digital converter (ADC).
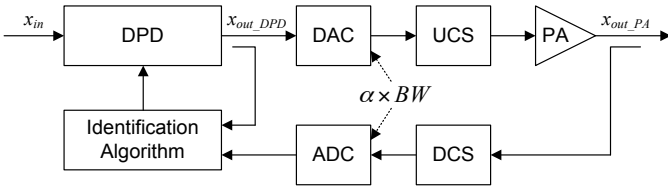

Fig. 3. Simplified block diagram of conventional DPD system.

In the system of Fig. 3, it is important to define the following parameters that are of primary interest in this work:

- *Signal bandwidth*: This refers to the bandwidth of the signal to be transmitted which is applied at the input of the predistorter.

- *DPD correction bandwidth*: This refers to the signal bandwidth at the output of the PA over which a spectrum regrowth reduction is observed following the use of the DPD.

- *Signal generation bandwidth*: This refers to the bandwidth of the signal applied at the input of the digital to analog converter in the signal generation path.

- *Signal observation bandwidth*: This corresponds to the bandwidth of the signal at the input of the analog to digital converter in the signal feedback path.

In the general case, the spectrum regrowth observed at the output of power amplifiers spans over a bandwidth α times wider than that of the input signal. In wireless infrastructure applications, the bandwidth of the signal at the output of the nonlinear power amplifier is typically five times that of the signal to be transmitted [15][16]. Indeed, for such applications seventh and higher orders intermodulation products do not have any noticeable effect on the output signal. This is mainly due to the high PAPR nature of the test signals and to the linearity-efficiency trade off adopted during the design of the DPD linearized power amplifiers. Thus, in the remainder of the paper, it will be considered that $\alpha = 5$. Nevertheless, this does not restrict the generality of the proposed technique which is anticipated to lead to extended correction bandwidth independently of the value of α.

Accordingly, if the input signal bandwidth is BW, then the DPD correction bandwidth should be $5 \times BW$. To ensure such DPD correction bandwidth, conventional DPD systems similar to the one shown in Fig. 3 require the signal generation bandwidth as well as the signal observation bandwidth to be equal to the DPD correction bandwidth, that is $5 \times BW$. With the adoption of wideband multi-carrier communication signals as it is the case in the LTE-A standard, digitally predistorted power amplifiers should be able to handle broadband input signal bandwidths obtained through carrier aggregation of a plurality of 20MHz wide signals. Even though LTE-A signals can have bandwidths as wide as 100MHz, bandwidths beyond 60MHz are commonly obtained through carrier aggregation between several frequency bands since typical frequency bands are only 60MHz wide (for example the 1930MHz to 1990MHz, or the 2110MHz to 2170MHz frequency bands). Since this work mainly focuses on single band power amplifiers predistortion, the maximum input signal bandwidth that will be considered will be limited to 60MHz. In such a case, the DPD correction bandwidth should be 300MHz wide. Consequently, the speed of the digital to analog converter as well as the analog to digital converter used in the system of Fig. 3 must be commensurate to this correction bandwidth (300MHz). For the ADC and DAC, the wide bandwidth constraint adds up to the dynamic range specifications required to ensure satisfactory adjacent channel performance of the linearized amplifier. This limits the correction bandwidth of state of the art digital predistortion systems as well as commonly used experimental setups to approximately 160MHz. This bandwidth translates into a signal bandwidth in the range of 30MHz which is not sufficient for LTE-A systems.

Based on the above discussion, the conventional DPD system of Fig. 3 has been modified to implement the proposed digital predistortion system with extended correction bandwidth. Herein, extended correction bandwidth refers to the fact that the DPD correction bandwidth exceeds its observation bandwidth as it will be demonstrated in the experimental validation section. Fig. 4 shows the simplified block diagram of the proposed bandwidth extended DPD system. In the proposed system, the digital predistortion is performed in two successive steps. First, the memoryless DPD synthesized from narrow band measurements is applied. Then, the input of the static nonlinear predistortion function and the

output of the PA are used by the DPD identification algorithm to build the dynamic nonlinearity compensation function. Thus, the system to be linearized in the second predistortion step is the cascade of the memoryless DPD function and the PA. As explained above, this system is a mildly nonlinear dynamic system that has memory effects comparable to that of the PA but significantly less static distortions. This contrasts with the highly nonlinear dynamic system being linearized in the conventional DPD architecture which is the PA itself. In other words, by using the memoryless nonlinear function, the system to be linearized is changed from being a highly nonlinear dynamic system (in the conventional DPD case) to a mildly nonlinear dynamic system (in the proposed bandwidth extended DPD) while the PA remains unchanged. Based on this, a lower sampling rate can be used in the analog to digital converter of the feedback path since the signal at its input has a bandwidth denoted $\beta \times BW$ with $\beta < \alpha$.
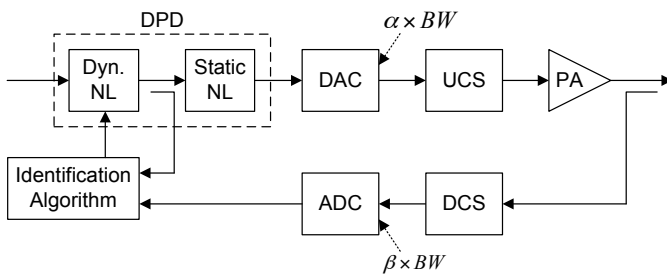

Fig. 4. Simplified block diagram of proposed bandwidth extended DPD system.

In the proposed bandwidth extended DPD system, two considerations need to be addressed: the synthesis of the static nonlinear DPD, and the unequal sampling rates of the signals fed to the dynamic distortions DPD identification algorithm block.

The static nonlinear function of the DPD is built in order to compensate for the memoryless distortions of the power amplifier. Since these distortions can be characterized from narrow band measurements and are primarily a function of the input signal's average power, it is possible to pre-synthesize these offline. For example, the static nonlinear DPD can be made of several functions indexed by the operating average power of the signal. Delay and power alignments are required for the static predistortion function synthesis as it is common for all predistortion systems. The alignments are performed offline since the static predistortion function is pre-synthesized from narrow band measurements. Furthermore, the architecture of the proposed DPD is robust to mismatches between the static nonlinearity of the DPD and the actual memoryless distortions of the PA since the dynamic nonlinearity function of the predistorter will compensate for any residual nonlinearities present in the cascaded system made of the PA and the DPD's static nonlinear function. Due to the sequential nature of the proposed approach, the static nonlinear predistortion function is considered to be part of the DUT being linearized by the dynamic nonlinear predistortion function; therefore, no specific power alignment is needed between these two predistortion functions and only power alignment is necessary at the input of the dynamic nonlinearity

block as it is the case in any predistortion system. Though, similarly to the case of the static nonlinear predistortion function, the dynamic nonlinear predistortion function involves time delay alignment between the two signals fed to the identification algorithm block of Figure 4. This time delay estimation and alignment is performed digitally using the cross-correlation technique described in [22], where the identification signals are resampled in order to improve the time resolution of the cross-correlation.

The signal at output of the feedback path's ADC has a sampling rate lower than that of the signal at the input of the DPD's static nonlinear function. Since both signals are used to identify the dynamic nonlinear function of the DPD, equal sampling rates are needed. To overcome this issue, the first step of the dynamic predistorter identification algorithm performs an oversampling of the ADC's output signal to have coherent sampling rates for both signals used to identify the dynamic distortions function of the DPD.

The flow chart describing the various steps involved in the bandwidth extended DPD system is reported in Fig. 5. First, the static nonlinear predistortion function derived from offline narrowband measurements is applied. Then, the input and output baseband waveforms of the cascade made up of the static DPD and the PA are acquired. The ADC's output signal is then up-sampled to the same sampling frequency as the input signal of the static DPD. The up-sampled output signal and the input signal are time aligned and then used to derive the coefficients of the dynamic nonlinear predistortion block.

In this work, all digital predistorters were built using the indirect learning architecture [23] where the input and output of the DUT are used to derive the post-inverse function which is then applied as a predistorter. This architecture is commonly adopted in adaptive digital predistortion systems. It is considered as an open loop system since the digital predistorter is outside the estimation loop. Thus, it is immune against propagation delay through the feedback path as long as delay estimation and alignment is performed prior to the digital predistortion function identification.
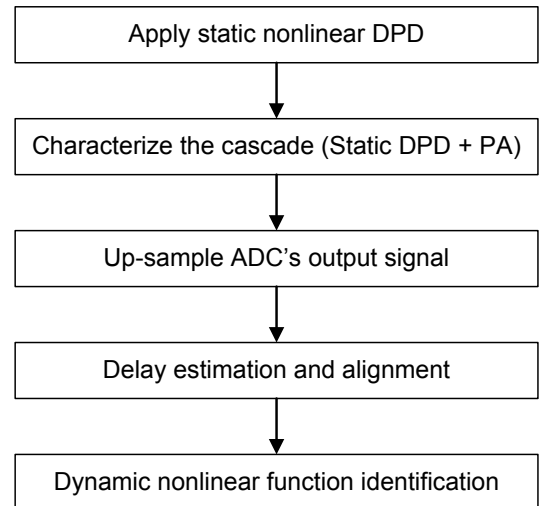

Fig. 5. Flow chart of the bandwidth extended DPD algorithm.

IV. EXPERIMENTAL VALIDATION

A. Experimental Setup

The experimental validation was carried using a 3-carrier LTE-A signal having a total bandwidth of 60MHz and a peak to average power ratio of 10.4dB at a complementary cumulative distribution function (CCDF) of 0.001%. To validate the proposed bandwidth extended DPD system, an experimental setup with wideband signal generation and analysis bandwidth (of more than 300MHz) was used. This will allow for comparison between the performance of the conventional and the proposed digital predistortion system for a wide range of signal observation bandwidths. In the experimental setup illustrated in Fig. 6, an arbitrary waveform generator (AWG) model 81180A from Agilent Technologies is used to generate baseband analog waveforms of the in-phase (I) and quadrature (Q) components of the test signal. These waveforms are modulated around the RF carrier frequency using the performance signal generator (PSG) model E8267D from Agilent Technologies. The RF signal is then applied at the input of the device under test. The resulting output is first attenuated and then demodulated using the Agilent 89600 vector signal analyzer (VSA) software running on a high speed oscilloscope model MSO 9404A from Agilent Technologies. The signal obtained at the output of the oscilloscope as well as the digital waveforms downloaded into the AWG are processed using MATLAB based algorithms to generate and apply the predistortion function in accordance with the conventional approach shown in Fig. 3. Herein, the digital predistortion functions are implemented within the data processing software. The ADC speed requirements are defined by setting, in the oscilloscope, the sampling rate of the PA's output signal.

The DUT used in this work is a high power Doherty power amplifier designed for operation in the 2100MHz frequency band (2110-2170 MHz). The measured AM/AM and AM/PM characteristics of the DUT driven by the 3-carrier LTE-A test signal are shown in Fig. 7. The shape of these characteristics reveals the highly nonlinear behavior of the DUT, and their dispersion exposes its strong memory effects.

During the tests, the power amplifier was operating over its entire power range at an output power back-off that is equal to the peak to average power ratio of the input signal (10.4dB). This leads to an operating average drain efficiency of 39%.
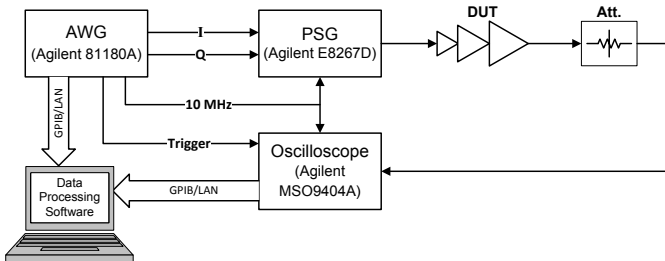

Fig. 6. Block diagram of the experimental setup.

B. Memoryless DPD Performance

To confirm that the observation bandwidth required at the output of the nonlinear power amplifier is five times that of the input signal, the spectra of the DUT's input and output signals were measured over a wide frequency span. These spectra depicted in Fig. 8 clearly confirm that the bandwidth of the signal at the output of the nonlinear power amplifier is 300MHz centered around the carrier frequency of 2140MHz (from 1990MHz to 2290MHz), and that intermodulation products beyond that of the fifth order are not observed at the output of the DUT.
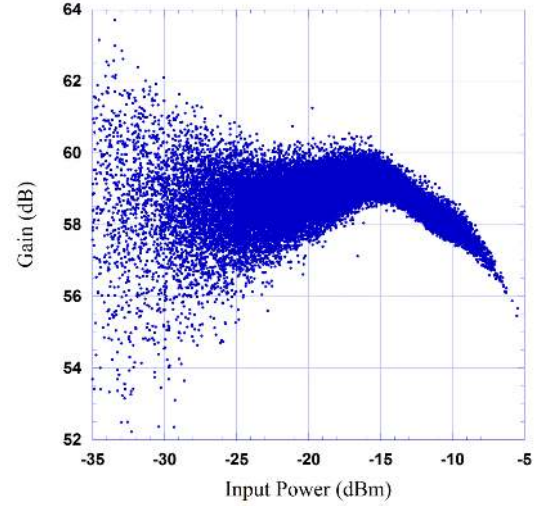
(a)
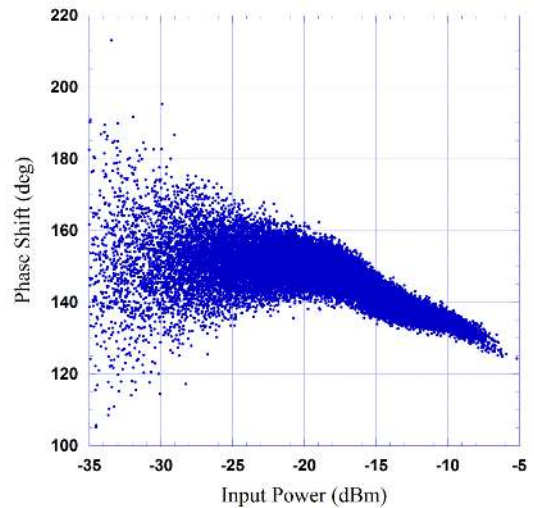
(b)

Fig. 7. Measured characteristics of the DUT using a 3-carrier LTE-A signal. (a) AM/AM characteristic. (b) AM/PM characteristic.

To experimentally validate the claims of section III according to which the use of a memoryless DPD will reduce the bandwidth requirements of the signal observation path, a memoryless DPD was derived from narrow band measurement of the DUT. In this test, the signal bandwidth was set to 20MHz, and accordingly the bandwidth of the signal observation path was set to 100MHz. The measurement data was used to generate a look-up table based (LUT) memoryless DPD of the DUT. This LUT was then applied to linearize the DUT driven by the 60MHz 3-carrier LTE-advanced signal centered around 2140MHz. The measured spectra at the output of the DUT with and without predistortion are shown in Fig. 9.

This figure clearly shows that the use of the memoryless predistorter significantly reduces the spectrum regrowth in the frequency range corresponding to the fifth order inter-modulation distortions (that is from 1990MHz to 2050MHz, and from 2230MHz to 2290MHz). To further corroborate this, the AM/AM and AM/PM characteristics of the cascade made of the LUT DPD and the DUT were measured. These curves reported in Fig. 10 confirm that the considered system (LUT DPD + DUT) is a mildly nonlinear dynamic system. Indeed, the nonlinearity of these characteristics has been significantly reduced as compared to their versions shown in Fig. 7, while the memory effects strength remains quasi unchanged as it can be observed through the dispersion of these characteristics.

As a conclusion, these results confirm that the use of the static DPD cancels out most of the nonlinearity exhibited by the DUT. Consequently, it reduces the bandwidth of the signal at the output of the PA. As a result, a lower sampling rate can be used in the signal observation path.
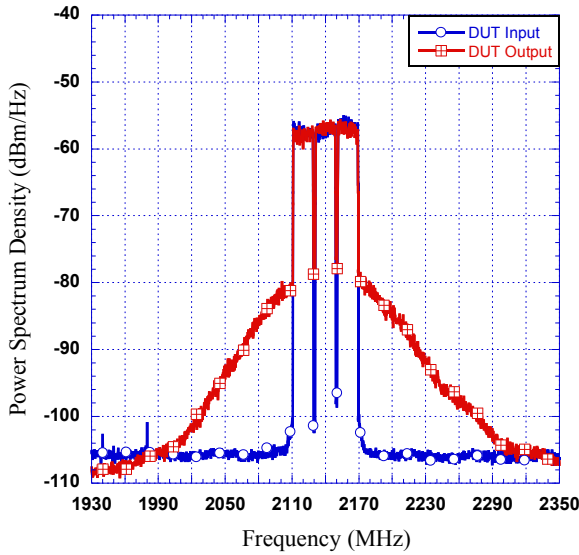

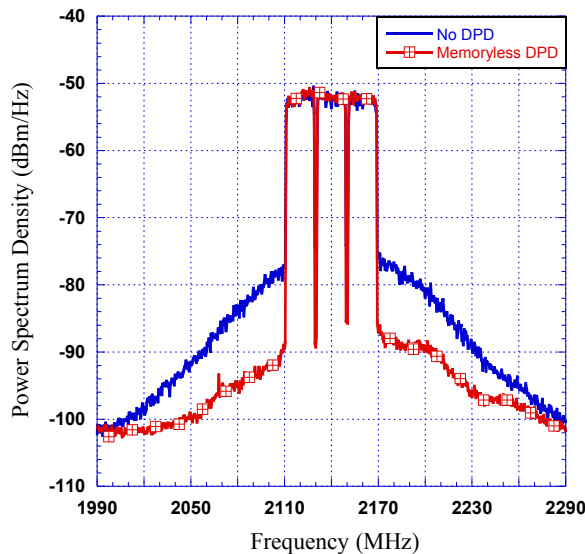Fig. 8. Measured spectra at the input and output of the nonlinear PA.

Fig. 9. Sample spectra at the output of a linearized PA.

C. Performance of the Proposed Bandwidth Extended DPD

To evaluate the effectiveness of the proposed technique in extending the bandwidth of digital predistortion systems, the DUT was linearized using the bandwidth extended DPD (BE-DPD) system as well as a conventional DPD (C-DPD) system. For fair comparison, in both cases, the structure of the DPD and its parameters were the same. In fact, the memoryless digital predistortion function was built using a look-up table while the dynamic nonlinear predistortion function was implemented using a memory polynomial function with a nonlinearity order of 5 and a memory depth of 10.

(a)

(b)
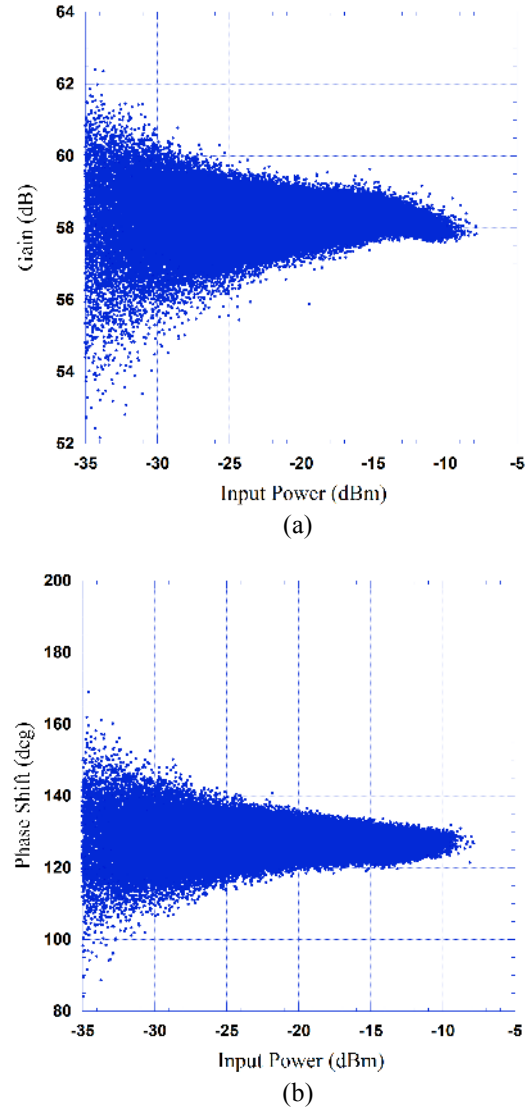
Fig. 10. Measured characteristics of the cascade (memoryless DPD+DUT) using a 3-carrier LTE-A signal. (a) AM/AM characteristic. (b) AM/PM characteristic.

Both the conventional and the proposed digital predistortion systems were experimentally validated for a wide range of signal observation bandwidths. In the C-DPD system, both static and dynamic predistortion functions are derived for each signal observation bandwidth. Conversely, for the proposed BE-DPD, the static nonlinear predistortion function is derived from narrow band measurements as described in the previous section and maintained unchanged during all tests. However,

the dynamic predistortion function is derived for each of the considered signal observation bandwidths.

Fig. 11 reports the spectra measured at the output of the linearized DUT using both techniques when the signal observation bandwidth is large enough to include the complete third and fifth order intermodulation products. This figure shows that, as expected, both the C-DPD and the BE-DPD lead to the same quality of linearization. In this test, the ADC sampling frequency was set to 384MHz. This sampling frequency corresponds to an observation bandwidth of 300MHz for the test equipment used in this experiment. The reference DPD refers to the single box predistorter built using a memory polynomial function derived from the characterization of the DUT using an observation bandwidth of 300MHz.
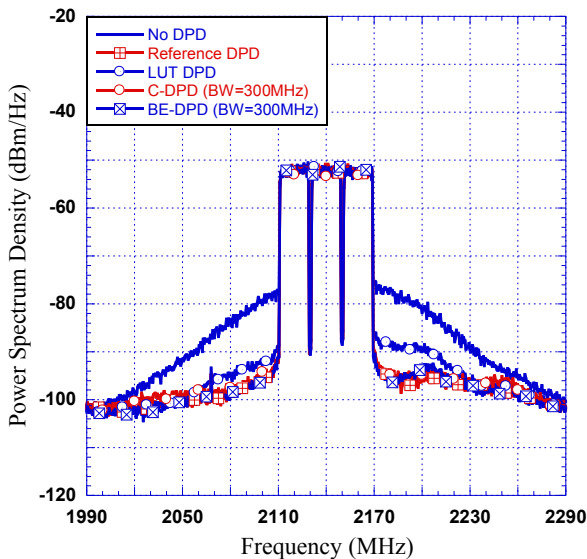

Fig. 11. Measured spectra at the output of the linearized DUT using 300MHz signal observation bandwidth.

The performances obtained for reduced signal observation bandwidth are presented in Fig. 12. In this figure, the spectra measured at the output of the linearized power amplifier are reported as a function of feedback path's ADC sampling frequency. This figure shows that for a sampling frequency of 276MHz, the performance of the C-DPD starts deviating from that of the reference DPD. The performance of the C-DPD further degrades as the ADC sampling frequency is reduced. Conversely, even if the ADC sampling frequency is reduced down to 184MHz, the performance of the proposed BE-DPD remains quasi unchanged. From these measurements, it appears that the BE-DPD can maintain a correction bandwidth of 300MHz even if the ADC sampling rate is reduced to 184MHz. This represents approximately 33% reduction of the necessary observation bandwidth required for C-DPD. In other words, the BE-DPD with an ADC sampling rate of Fs can achieve the same correction bandwidth as a conventional DPD system with a sampling rate 50% higher $(1.5 \times Fs)$.

As the sampling rate, and thus the observation bandwidth, was further reduced gradually from 184MHz down to 123MHz. The spectra presented in Fig. 12 (e) and (f) show that the performance of the C-DPD and BE-DPD are affected.

Here, it is essential to note that even under such conditions, the performances of the propose BE-DPD remain superior to that of the C-DPD. In fact, the degradation of the BE-DPD performance is upper bounded by the performance of the LUT DPD. This means that as the ADC sampling rate of the feedback path is reduced, the BE-DPD performance will converge to that of the LUT DPD. This contrasts with the C-DPD case for which the spectrum regrowth in the frequency range outside the signal observation bandwidth is similar to that obtained without DPD. These results clearly demonstrate the ability of the BE-DPD to outperform the C-DPD even under extreme bandwidth constraints.

V. CONCLUSION

In this paper a bandwidth extended digital predistortion system was proposed. This system is based on a two-box digital predistorter architecture in which the static predistortion function is derived offline under narrow band test conditions and a memory polynomial DPD is then applied to linearize the cascade made of the static DPD and the device under test. The use of the static DPD was shown to reduce the spectrum regrowth at the output of the linearized DUT which in turn reduces the observation bandwidth requirements needed for the synthesis of the memory polynomial predistortion function. Experimental results using a 3-carrier LTE-A signal demonstrated the ability of the proposed BE-DPD in achieving satisfactory linearity performance over a 300MHz bandwidth with a sampling rate of 184MHz in the feedback path's ADC.

REFERENCES

[1] F. H. Raab, P. Asbeck, S. Cripps, P. B. Kenington, Z. B. popovic, N. Pothecary, J. F. Sevic, and N. O. Sokal, "Power amplifiers and transmitters for RF and microwave," *IEEE Trans. Microw. Theory Tech.*, vol. 50, no. 3, pp. 814-826, Mar. 2002.

[2] W. Chen, S. Zhang, Y. Liu, Y. Liu, and F. M. Ghannouchi, "A concurrent dual-band uneven Doherty power amplifier with frequency-dependent input power division," *IEEE Trans. Circuits Syst. I, Reg. Papers,* vol. 61, no. 2, pp. 552-561, Feb. 2014.

[3] A. M. M. Mohamed, S. Boumaiza, and R. R. Mansour, "Electronically tunable Doherty power amplifier for multi-mode multi-band base stations," *IEEE Trans. Circuits Syst. I, Reg. Papers,* vol. 61, no. 4, pp. 1229-1240, Apr. 2014.

[4] R. Darraji and F. M. Ghannouchi, "RF/DSP codesign methodology of enhanced Doherty amplifiers," *IEEE Trans. Circuits Syst. II, Exp. Briefs,* vol. 59, no. 4, pp. 219-223, Apr. 2012.

[5] Y. Li, J. Lopez, D. Y. C. Lie, K. Chen, T. Y. Zhang, and G. K. Ma, "Circuits and system design of RF polar transmitters using envelope-tracking and SiGe power amplifiers for Mobile WiMAX," *IEEE Trans. Circuits Syst. I, Reg. Papers,* vol. 58, no. 5, pp. 893-901, May 2011.

[6] D. Kang, B. Park, D. Kim, J. Kim, Y. Cho, and B. Kim, "Envelope-tracking CMOS power amplifier module for LTE applications," *IEEE Trans. Microw. Theory Tech,* vol. 61, no. 10, pp. 3763-3773, Oct. 2013.

[7] H. Tango, T. Hashinaga, K. Totani, H. Kuriyama, Y. Hamada, and T. Asaina, "A 60% efficient envelope tracking power amplifier for 40W, 2.6GHz LTE base station with in/output harmonic tuning," *IEEE MTT-S International Microw. Symp.,* pp. 1-4, Jun. 2013.

[8] A. S. H. Ghadam, S. Burglechner, A. H. Gokceoglu, M. Valkama, and A. Springer, "Implementation and performance of DSP-oriented feedforward power amplifier linearizer," *IEEE Trans. Circuits Syst. I, Reg. Papers,* vol. 59, no. 2, pp. 409-425, Feb. 2012.

[9] H. H. Boo, S. W. Chung, and J. L. Dawson, "Digitally assisted feedforward compensation of Cartesian-feedback power-amplifier systems," *IEEE Trans. Circuits Syst. II, Exp. Briefs,* vol. 58, no. 8, pp. 457-461, Aug. 2011.
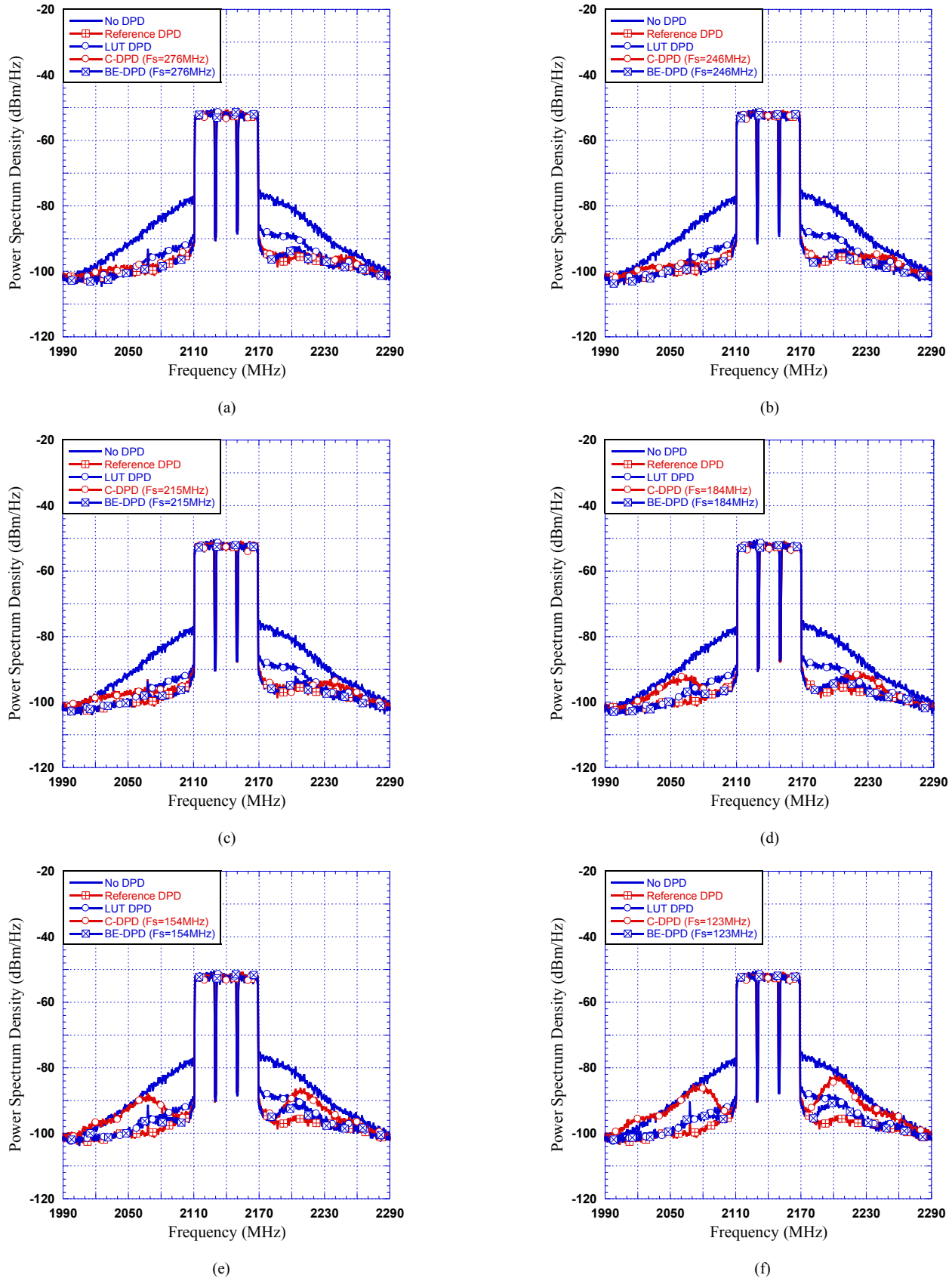
Fig. 12. Measured spectra at the output of the linearized DUT using the C-DPD and the BE-DPD for various ADC sampling rates. (a) Fs=276MHz, (b) Fs=246MHz, (c) Fs=215MHz, (d) Fs=184MHz., (e) Fs=154MHz, (f) Fs=123MHz.

[10] X. Yu and H. Jiang, "Digital predistortion using adaptive basis functions," *IEEE Trans. Circuits Syst. I, Reg. Papers,* vol. 60, no. 12, pp. 3317-3327, Dec. 2013.

[11] M. Younes and F. M. Ghannouchi, "On the modeling and linearization of a concurrent dual-band transmitter exhibiting nonlinear distortion and hardware impairments," *IEEE Trans. Circuits Syst. I, Reg. Papers,* vol. 60, no. 11, pp. 3055-3068, Nov. 2013.

[12] M. Rawat, F. M. Ghannouchi, and K. Rawat, "Three-layered biased memory polynomial for dynamic modeling and predistortion of transmitters with memory," *IEEE Trans. Circuits Syst. I, Reg. Papers,* vol. 60, no. 3, pp. 768-777, Mar. 2013.

[13] F. M. Ghannouchi and O. Hammi, "Behavioral modeling and predistortion," *IEEE Microw. Mag.*, vol. 10, no. 7, pp. 52-64, Dec. 2009.

[14] O. Hammi and F. M. Ghannouchi, "Twin nonlinear two-box models for power amplifiers and transmitters exhibiting memory effects with application to digital predistortion," *IEEE Microw. Wireless Compon. Lett.,* vol. 19, no. 8, pp. 530-532, May 2009.

[15] C. Yu, L. Guan, E. Zhu, and A. Zhu, "Band-limited Volterra series-based digital predistortion for wideband RF power amplifiers," *IEEE Trans. Microw. Theory Tech*, vol. 60, no. 12, pp. 4198-4208, Dec. 2012.

[16] Y. Ma, Y. Yamao, Y. Akaiwa, and K. Ishibashi, "Wideband digital predistortion using spectral extrapolation of band-limited feedback signal," *IEEE Trans. Circuits Syst. I, Reg. Papers,* vol. 61, no. 7, pp. 2088-2097, Jul. 2014.

[17] M. Seo, K. Kim, M. Kim, H. Kim, J. Jeon, M. K. Park, H. Lim, and Y. Yang, "Ultrabroadband linear power amplifier using a frequency-selective analog predistorter," *IEEE Trans. Circuits Syst. II, Exp. Briefs,* vol. 58, no. 5, pp. 264-268, May 2011.

[18] K. H. Lim, G. Ahn, S. Jung, H. C. Park, M. S. Kim, J. H. Van, J. H. Jeong, C. S. Park, and Y. Yang, "A 60-W multicarrier WCDMA power amplifier using an RF predistorter," *IEEE Trans. Circuits Syst. II, Exp. Briefs,* vol. 56, no. 4, pp. 265-269, Apr. 2009.

[19] O. Hammi, S. Carichner, B. Vassilakis, and F. M. Ghannouchi, "Power amplifiers' model assessment and memory effects intensity quantification using memoryless post-compensation technique," *IEEE Trans. Microw. Theory Tech.*, vol. 56, no. 12, pp. 3170-3179, Dec. 2008.

[20] O. Hammi, A. M. Kedir, and F. M. Ghannouchi, "Nonuniform memory polynomial behavioral model for wireless transmitters and power amplifiers," *IEEE Asia-Pacific Microwave Conf. (APMC2012)*, pp. 836-838, Dec. 2012.

[21] O. Hammi, S. Bensmida, and K. Morris, "Behavioral modeling of class J amplifier driven by 100MHz LTE-advanced signal using dynamic nonlinearity reduction," *IEEE Topical Meeting on Power Amplifiers for Wireless and Radio Applications (PAWR 2014)*, pp. 67-69, Jan. 2014.

[22] T. Liu, S. Boumaiza, and F. M. Ghannouchi, "Deembedding static nonlinearities and accurately identifying and modeling memory effects in wide-band RF transmitters," *IEEE Trans. Microw. Theory Tech.*, vol. 53, no. 11, pp. 3578-3587, Nov. 2005.

[23] L. Ding, G. T. Zhou, D. R. Morgan, Z. Ma, J. S. Kenney, J. Kim, and C. R. Giardina, "A robust digital baseband predistorter constructed using memory polynomials," *IEEE Trans. Commun.*, vol. 52, no. 1, pp. 159-165, Jan. 2004.

Oualid Hammi (S'03–M'09) received the B.Eng. degree from the École Nationale d'Ingénieurs de Tunis, Tunis, Tunisia, in 2001, the M.Sc. degree from the École Polytechnique de Montréal, Montréal, QC, Canada, in 2004, and the Ph.D. degree from the University of Calgary, Calgary, AB, Canada, in 2008, all in electrical engineering.

He is currently an Assistant Professor with the Department of Electrical Engineering, King Fahd University of Petroleum and Minerals, Dhahran, Saudi Arabia. From 2009 to 2010, he was a Post-Doctoral Fellow with the Intelligent RF Radio Laboratory (iRadio Lab), Schulich School of Engineering, University of Calgary. He has authored or co-authored over 70 publications, and is reviewer for several IEEE transactions. His research interests include the design of energy efficient linear transmitters for wireless communication systems and the characterization, behavioral modeling, and linearization of radiofrequency power amplifiers and transmitters.

Andrew Kwan (S'07) received the B.Sc. degree in computer engineering and M.Sc. degree in electrical engineering from the University of Calgary, Canada in 2006 and 2009, respectively.

He is currently working towards the Ph.D. degree in the iRadio Laboratory at the University of Calgary. His research interests include signal processing for wireless communications systems, power efficiency enhancement for RF transceivers, embedded systems, and software defined radios.

Souheil Bensmida received the MSc. degree in electronics and instrumentation from the University of Pierre and Marie Curie Paris 6, Paris, France, in 2000, and the Ph.D. degree in electronics and communications from the Ecole Nationale Supérieure des Télécommunications (ENST), Paris, France, in 2005. Between October 2006 and August 2008, he was a Post-Doctoral Fellow with the iRadio Laboratory, University of Calgary, Canada. He is now Research Associate at University of Bristol, UK. His research interest is the non-linear characterisation and linearisation of power amplifiers for mobile and satellite applications and microwave instrumentation.

Kevin A. Morris received his B.Eng. and Ph.D. degrees in electronics and communications engineering from the University of Bristol in 1995 and 1999 respectively. He currently holds the post of Reader in Radio Frequency Engineering within the Department of Electrical and Electronic Engineering at the University of Bristol. Currently he is involved with a number of research programmes within the U.K. He has authored or co-authored 60 academic papers and is the joint author of 5 patents. His research interests are principally in looking at methods of reducing power consumption in communications systems including the area of radio frequency hardware design with specific interest in the design of efficient linear broadband power amplifiers for use within future communications systems.

Fadhel Ghannouchi (S'84, M'88, SM'93, FIEEE' 07) is currently a professor and iCORE/CRC Chair at Electrical and Computer Engineering Department of The Schulich School of Engineering of the University of Calgary and Director of Intelligent RF Radio Laboratory (www.iradio.ucalgary.ca). His research interests are in the areas of microwave instrumentation and measurements, nonlinear modeling of microwave devices and communications systems, design of power and spectrum efficient microwave amplification systems and design of intelligent RF transceivers for wireless and satellite communications. His research activities led to over 600 publications and 15 US patents (5 pending) and three books.